New Journal of Physics
The open access journal at the forefront of physics

Deutsche Physikalische Gesellschaft DPG IOP Institute of Physics

PAPER • OPEN ACCESS

Beam formation in CERNs cesiated surfaces and volume H^- ion sources

To cite this article: Serhiy Mochalskyy *et al* 2016 *New J. Phys.* **18** 085011

IOP Publishing | New J. Phys. 18 (2016) 085011 | doi:10.1088/1367-2630/18/8/085011

New Journal of Physics

The open access journal at the forefront of physics

Deutsche Physikalische Gesellschaft DPG
IOP Institute of Physics

Published in partnership with: Deutsche Physikalische Gesellschaft and the Institute of Physics

CrossMark

OPEN ACCESS

RECEIVED
11 April 2016

REVISED
23 June 2016

ACCEPTED FOR PUBLICATION
5 July 2016

PUBLISHED
19 August 2016

PAPER

Beam formation in CERNs cesiated surfaces and volume H^- ion sources

Serhiy Mochalskyy[1], **Jacques Lettry**[2] **and Tiberiu Minea**[3]

[1] Max-Planck-Institut für Plasmaphysik, Boltzmannstr. 2, D-85748, Garching, Germany
[2] CERN-ABP, Genève, Switzerland
[3] Laboratorire de Physique des Gaz et des Plasma, CNRS, Univ. Paris-Sud, Université Paris-Saclay, F91405, France

E-mail: serhiy.mochalskyy@ipp.mpg.de

Keywords: CERN, negative ion source, PIC modeling, Monte Carlo modeling

Abstract

At CERN, a high performance negative ion (NI) source is required for the 160 MeV H^- linear accelerator named Linac4. The source should deliver 80 mA H^- ion beams within an emittance of 0.25 mm·mrad. For this purpose two ion sources were developed: IS01 is based on the NI volume production and IS02 provides additional NI by surface production via H interaction on a cesiated Molybdenum plasma electrode. The development of negative ion sources for Linac4 is accompanied by modelling activities. ONIX code has been modified and adapted to investigate the transport of NI and electrons in the extraction region of the CERN negative ion sources. The simulated results from modeling of IS01 and IS02 extraction regions, which were obtained in 2012 during source commissioning, are presented and benchmarked with experimental measurements obtained after 2013. The formation of the plasma meniscus and the screening of the extraction field by the source plasma are discussed. The NI production is compared between two types of sources, the first one based on volume production only and the second one encompassing NI cesiated surface production. For the IS02 source, different states of conditioning were simulated by changing the NI emission flux from the plasma electrode and Cs^+ density in the bulk plasma region. The numerical results show that in low work function regime, with high NI surface emission rate of 3000 A m^{-2} and Cs-density of $n_{Cs+} = 3.8 \times 10^{16}$ m^{-3}, the total extracted NI current could reach ~80 mA. At the less favorable Cs-coverage, when the surface NI emission rate becomes significantly lower, namely 300 A m^{-2} with $n_{Cs+} = 3.3 \times 10^{15}$ m^{-3}, the total extracted NI current only reaches ~20 mA. A good agreement between simulation and experimental results is observed in terms of extracted NI current for both extraction systems, including the case of reversed extraction potential that corresponds to positive (H^+) ion extraction.

1. Introduction

At CERN, the linear accelerator Linac4 is designed to accelerate negative hydrogen ions (NI) to 160 MeV energy [1]. In 2018–19, Linac4 will replace the 50 MeV proton linear accelerator (Linac2), injector to the Proton Synchrotron Booster (PSB). This is part of the upgrade of the Large Hadron Collider (LHC) [2] injector chain towards higher luminosity [1]. The negative ion source has to supply 80 mA of H^- beam within an emittance of 0.25 mm mrad that is technically very challenging and requires a deep understanding of the extraction mechanism and of the negatively charged plasma sheath.

Two NI ion sources were developed in the framework of the Linac4 project [2–4] and are illustrated in figure 1. The first one—IS01—is based on volume NI production only. A thin layer of cesium can be deposited on the molybdenum plasma electrode of the second ion source—IS02—by vaporization of metallic cesium. The low work function Cs-coated Mo-plasma electrode therefore contributes to the NI production via re-emission of a fraction of the proton and H_0 fluxes as negative ions. In both sources plasma is generated by an external 4–6

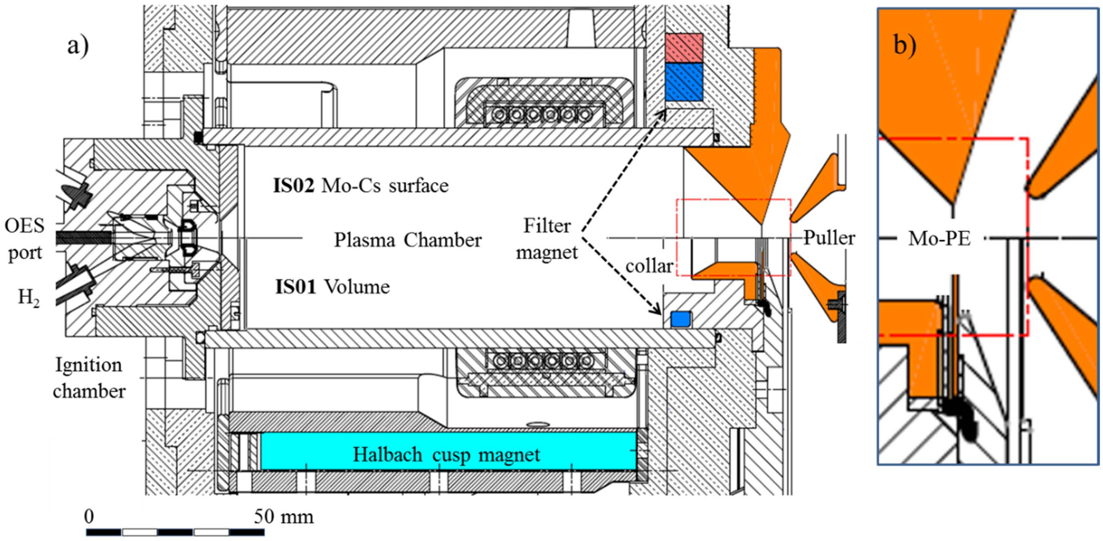

Figure 1. (a) Comparative view of the negative ion source plasma chambers designed for Linac4, IS01 (bottom half) operates in volume and IS02 (top half) in cesiated surface H^- production mode. The axis corresponds to the cylindrical symmetry axis. The puller electrode (orange) is shown and the region of PIC simulation is indicated with a dash-dotted line. (b) Detail view of the Molybdenum plasma electrodes.

turns solenoid operated at 2 MHz and powered up to 100 kW which ignites and heats the hydrogen plasma [2, 5]. The plasma chambers are made of aluminum oxide or nitride (Al_2O_3, AlN) ceramic of inner and outer diameters of 48 mm and 64 mm, respectively [4]. A permanent magnet octupole in Halbach configuration is installed around the plasma chamber and generates a magnetic field cusp structure [6]. A dipole filter field separates the inductive plasma heating region where excited hydrogen molecules are produced form the beam formation region where low energy electrons contribute to the dissociative attachment process [7]. Negative ions are extracted by biasing the puller electrode with respect to the plasma chamber.

The extraction apertures used in IS01 and IS02 sources are illustrated in figure 1, (orange color), IS01 has a cylindrical shape and the IS02 has a double chamfered conical plasma electrode. The extraction aperture diameter is 6.5 mm and the distance with respect to the puller electrode is 7 mm. The IS01 aperture can be biased against the plasma in order to decrease the co-extracted electron current.

In the IS01 source, hydrogen NI are produced via so called 'volume production' channel based mainly by the dissociative low energy electron (~1 eV) attachment to high vibrational states hydrogen molecules ($H_2(v) + e \rightarrow H + H^-,\ v > 5$) [7]. However, this attractive mechanism faces a variety of loss processes driven by more energetic electrons or ions [7, 8]. Consequently, the extracted NI current density using the volume production mechanisms only is relatively low (<30 mA) [2]. To overcome this limitation and to reduce the amount of co-extracted electrons, the IS02 source operates in the 'surface production' mode. Hence, the surface of the plasma electrode is covered with Cs atoms to activate this NI production mechanism [9, 10]. Evaporated Cs atoms stick to the Mo-surface and their ability to release electrons towards the impinging hydrogen atom depends on the coverage fraction of the surface. The highest contribution to the NI beam formation originates from the surfaces close to the extraction electrode. Two processes occur via surface conversion, (i) simple electron capture on impinging atoms ($H + e_{\mathrm{surface}} \rightarrow H^-$) and (ii) double electron capture on positive ions ($H^+ + e_{\mathrm{surface}} \rightarrow H;\ H + e_{\mathrm{surface}} \rightarrow H^-$). The Cs coverage determines the effectiveness of the H conversion in NI, but impurities degrade the work function, which governs the NI emission rate from the surface. The IS02 ion source is operated with periodical hydrogen free Cs-injection at typically 30 days intervals, followed by a few hours of conditioning with plasma in the absence of extraction field. At the beginning of the conditioning period, we observe a low NI surface production yield reflected by the low ion current density extracted and high electron current. After conditioning, a large negative ion emission rate from the cesiated surface leads to high extracted NI current.

Besides the increase of the H^- extracted current, it is important to minimize the amount of co-extracted electrons. Co-extracted electrons induce heat loads on the electron dumping system and contribute to increasing the beam emittance. Simultaneous increase of the NI and reduction of the electron current passing through the aperture is a source design challenge and requires in depth analysis of the beam formation and extraction regions.

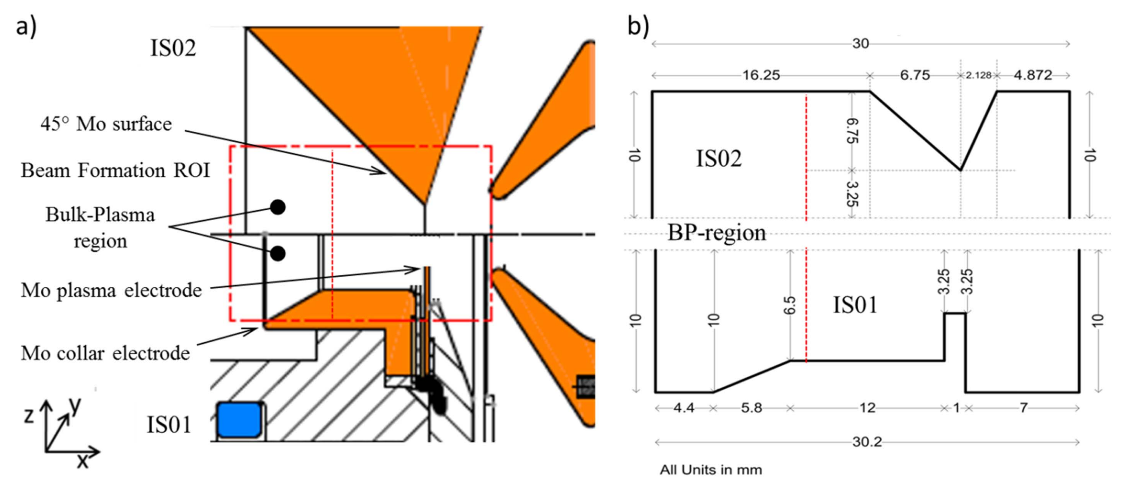

Figure 2. (a) Detailed sketch of the Linac4 beam formation region for H^- volume production (IS01) and cesiated surface production (IS02). The extraction aperture is 6.5 mm diameter for both sources and the distance from the center of the aperture to the 25 kV puller electrode is 7mm. The simulation domain is indicated by the dash-dotted line. (b) Schematic view of the simulation domains used in the ONIX code (x–y mid plane) for modeling IS01 (bottom) and IS02 (top) extraction systems. The end of the bulk plasma region $[0 > x > 12.3]$ is indicated with a vertical dotted line.

The size of the aperture, the current densities (electron and NI), and the complex three dimensional (3D) structures of the electric and magnetic fields in the extraction region, prevent the use of known diagnostic techniques to measure local plasma parameters. Numerical simulation, which includes realistic source parameters, will provide insight to the formation of the sheath (the region where charge separation appears) and seems to be the unique approach capable of describing the 3D behavior of the plasma and beam formation. The simulated NI beam can be compared to experimental results collected downstream from the extraction region and gives important hints for future source optimization by understanding the processes governing the particle transport and meniscus formation.

In order to model the negative ion extraction and the plasma behavior in the vicinity of the extraction aperture the modified version of the self-consistent 3D particle-in-cell (PIC) Monte Carlo Collisional (MCC) code named ONIX has been used. Details about this model are given in the next section and in [11]. This work is focused on the general description of both extraction systems developed at CERN and benchmark of the simulation results with measured data from these sources. The self-consistent positive ion meniscus formation is shown together with the screened potential distributions. The extracted NI and co-extracted electron currents are analyzed for different plasma and source operation conditions. Finally, the NI extracted current resulting from volume and Cs-surface production mechanism of IS02 is analyzed and compared to the one resulting from volume production.

This paper is structured as follow: section 2 details the numerical features and background of the ONIX model. The obtained results and cross-checked analysis is presented and discussed in section 3. The last section summarizes the main conclusions of this work and describes the possibilities for future work.

2. Simulation model

3D particle-in-cell Monte Carlo Collision electrostatic code ONIX (Orsay Negative Ion eXtraction) was initially developed in the laboratory LPGP, Orsay, France in order to simulate the particle transport in the electronegative plasmas, in the vicinity of the extraction electrode of an ITER-like NI source extraction system [11, 12]. The initial conditions consist of a homogeneous bulk plasma covering the first 12.3 mm of the simulation domain, i.e., the uniform plasma slice situated the furthest with respect to the extraction aperture (figures 2 and 6(a)). The geometry of the extraction electrode, the fields (electric and magnetic), as well as the ability of the surfaces to release charged particles (surface emission rate) are taken into account as realistically as possible. The last version of ONIX allows the use of a direct current bias on the extraction electrode with respect to the plasma [13]. A detailed description of ONIX can be found in [14, 15], however, the main features of the model are recalled here-below.

The code was adapted and improved to simulate the extraction system of the IS01 and IS02 NI source testbeds with the 3D geometry of the extraction electrodes, realistic 3D magnetic field configuration [16], and Cs^+ ions in the bulk plasma region. Let us note that previous works concerning ITER-like simulations

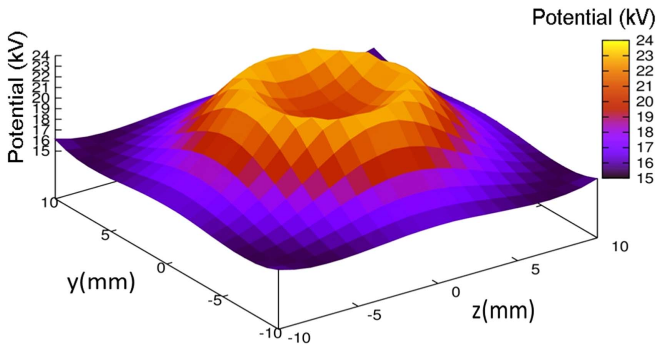

Figure 3. Input potential 2D distribution at the right hand side boundary of the simulation domain calculated using the real puller geometry by the commercial OPERA 3D package.

[11, 12, 14, 15] consider periodic boundary conditions of the simulation volume in the two directions orthogonal to the NI beam axis. Hence, the previous simulation results correspond to an infinite 2D plasma grid; the total current passing through this grid being estimated as the extracted current through one aperture multiplied by the total number of apertures of the grid. When compared to fusion sources, the particularity of the CERN NI source consists of a single extraction aperture. Hence, the simulated electron and NI beam currents are directly comparable to measurements. While ONIX was validated against other codes and experimental results from the BATMAN NI source test bed [14, 15], the opportunity to compare ONIX results with ones from a high density plasma accelerator ion source is taken as a challenge.

Two simulation domains have been implemented in ONIX corresponding to the extraction systems IS01 and IS02 (figure 2(a)). The simulation volumes include the extraction aperture of 6.5 mm diameter and have spatial dimensions of 30 mm $\times$ 20 mm $\times$ 20 mm in x, y, z directions, respectively (figure 2(b), x—is the symmetry axis). The main difference between these two simulation domains is the aperture's shape: in the IS01 system it is represented by a 1 mm wide cylinder, whereas in IS02 it is double chamfered as two cones with joint bases and 3.25 mm inner radius (figure 2(b)).

In comparison to the previous version of ONIX code [11], the boundary conditions were changed in order to match the experimental set up of IS01 and IS02. They assume now perfect metal walls surrounding the box in y and z directions and left hand side wall (figure 2(b)). In the CERN version of ONIX, all plasma particles that strike these boundaries are reinjected in the bulk plasma since the boundary condition is not periodic (i.e., the walls are assumed perfect absorbers).

The potential distribution in the whole 3D volume is calculated as the solution of the Poisson's equation ($\nabla^2\varphi = -\rho/\varepsilon_0$). The iterative Preconditioned Conjugate Gradient method [17] is used to solve this equation. In order to get the realistic potential distribution in the vicinity of the extraction aperture, which has a circular cross section, special techniques are implemented in the Poisson solver to deal with domain boundaries lying between mesh nodes [12, 18]. The Dirichlet condition is referred to all solid wall boundaries of the simulation domain with constant potential value. The extraction potential is applied only to the right boundary of the simulation domain (after the extraction aperture). This potential distribution at the boundary of the simulation domain in a plane orthogonal to the beam axis is due to the puller electrode and shown in figure 3. It was calculated without plasma (in vacuum, i.e., $\rho = 0$) using the real 3D puller geometry with the OPERA 3D package [19]. The rest of the domain boundaries are assumed to be grounded ($V = 0$). Very good agreement has been found for the potential distribution in vacuum, between OPERA calculations and the ONIX code results (not shown).

In ONIX, the electric field is calculated from the potential distribution at the secondary mesh using potential values calculated from Poisson solver ($E = -\nabla V$). In the previous version of the model [11] one value of the E field component was calculated by using two potential points at the two nearest PIC nodes ($E_n = -(V_{n+1} - V_n)/\Delta x$). A significant change is implemented in this version of the numerical model to describe the much higher (more than one order of magnitude) plasma density generated in IS01 and IS02 in comparison to the fusion NI sources. The higher the density, the higher the numerical noise (fluctuation of the potential and the electric field). Each macro particle represents 5×10^5 real particles. The electric field is interpolated over 64 PIC nodes (Cloud-in-Cell) [20] for the 3D case. Figure 4 shows the electric field distribution along the axial direction using different number of nodes for calculating one component of the electric field. Extending the derivative calculation to 18 PIC nodes (red line on figure 4), the distribution becomes smoother suppressing artificial peaks and avoiding the eventual numerical heating of the plasma electrons but preserving the main features of the electric field.

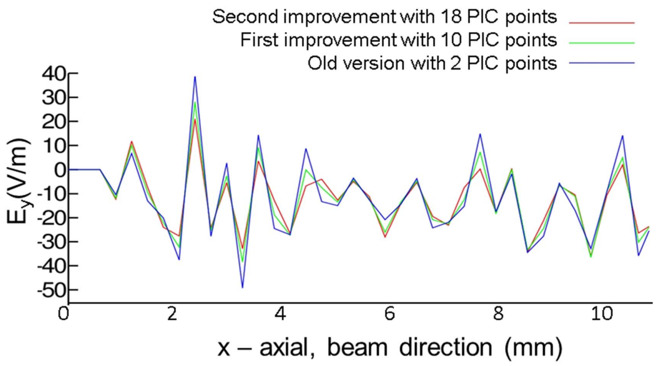

Figure 4. Electric field distribution in the axial direction (x) at the mid z-y plane. Blue line corresponds to the initial calculation algorithm using the two nearest PIC nodes, green line represents the subroutine version using the 10 nearest PIC points (in 3D) and red line shows the used version of the routine for CERN calculations of the electric field using 18 potential PIC nodes (in 3D). The range of 10 mm corresponds to the 33 PIC nodes.

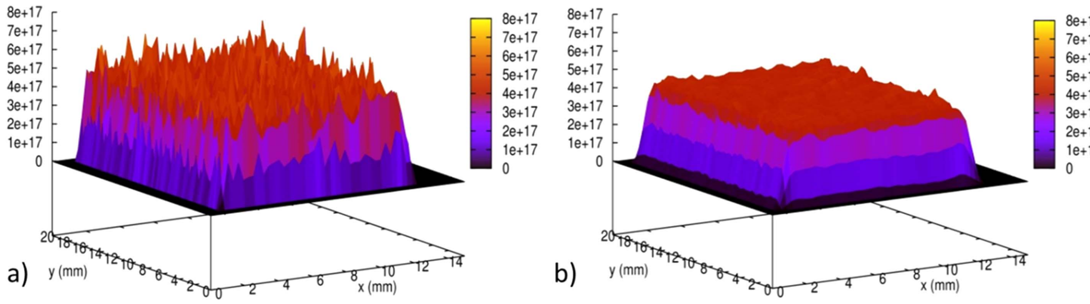

Figure 5. Initial electron density distribution using 8 (a) and 64 (b) PIC nodes in the charge assignment routine, for a total plasma density of 5×10^{17} m^{-3}.

For a stable plasma simulation using an explicit algorithm, which is the case here, the chosen time step should be smaller than the inverse plasma frequency and the size of the PIC cell should be smaller than the Debye length. In addition to these basic criteria the most important condition, known as the CFL (Courant Friedrichs Lewy) stability criterion [21], must be fulfilled. In current simulations, a typical run is performed using ~20 million macro particles with a meshing of $110 \times 100 \times 100$ PIC nodes. The code performance is ~0.1 μs per day on 20 CPUs with the time step $\Delta t = 3 \times 10^{-12}$ s $< 1/\omega_p \sim 1.77 \times 10^{-11}$ s. Let us note that ONIX simulation deals with the extraction (sheath) region, so even if the cell size is slightly larger than Debye length the most important CFL criterion is always satisfied. In order to decrease the numerical heating that could arise from high plasma density, in addition to the new electric field calculation subroutine described above, the second order charge assignment onto the PIC nodes has been specially developed for this case known also as Claud-in-Cell (CIC) approach. The advantage of this novel algorithm is shown in figure 5 where the initial electron density distribution is shown (a) for initial first order projection procedure using 8 nearest PIC nodes and (b) for the new second order projection procedure using 64 PIC nodes, used for CERN simulations. One can clearly see that the charge density spikes present on figure 5(a) have disappeared on figure 5(b), drastically reducing the numerical heating. Moreover, test simulations with different number of macro particles per cell have been done to prove the absence of the significant influence of the numerical noise. It was found that simulations of 50 particles per cell (standard ONIX set up) give similar results as 150 particles per cell for the extracted current, potential and charge density distribution. Therefore, realistic 3D simulations with a plasma density as high as $n_e = 10^{18}$ m^{-3} have been performed with the improved version of ONIX.

The simulations input data have been systematically chosen as close as possible to the experimental conditions. The plasma density and temperature far from the extraction aperture are considered uniform and some of these values were taken from the experiments [22–24] or were assumed based on the know-how accumulated via the previous modeling of other RF high density NI sources [9, 11]. The initial plasma (given parameters, density, temperature) is assumed in the left side of the simulation domain ($0 < x < 12.5$ mm—figure 2(b)) and it is composed of H^+, H_2^+, H_3^+, H^- and electrons. In the latest development Cs^+ ions were also introduced as plasma species. The plasma neutrality is maintained in the reservoir region by re-injection of the same species of particle if it leaves (destroyed or extracted) the simulation domain. The density was set to $n_0 = 10^{18}$ m^{-3} for the positive and negative species with the source ratio: $S_{H^+}/S_{H_2^+}/S_{H_3^+} = 0.7/0.2/0.1$; $S_e/S_{H^-} = 0.5/0.5$. The initial electron temperature was set to $T_e = 5$ eV, whereas the ions temperature was taken 1.5 eV. ONIX assumes a uniform density of the neutral gas background, that is reasonable for a relatively weak ionization degree (<5%) with constant density $n_H = 10^{20}$ m^{-3} and temperature $T_H = 0.75$ eV.

A full 3D magnetic field map of the cusp system has been calculated by using the TOSCA module of the OPERA software package [19], which uses finite element methods to solve magnetostatic problems. Obtained field distributions for the ONIX simulation domain were implemented in the model. To do this, the **B**-field firstly is interpolated on the PIC grid nodes and after on the particles position, in the charged particle pusher routine.

The Monte Carlo Collision module in the ONIX code includes the self-consistent NI production in the volume via electron dissociative attachment to the vibrationally exited molecules $H_2(v)$. The complete list of the most important NI destruction processes is detailed in [11]. Electron elastic collision ($e + H \rightarrow e + H$) has been added to this kinetic module due to the importance of this elementary process not necessarily for the electron energy transfer but for the scattering effect that reduces the co-extracted electron current. The NI production at the cesium covered extraction electrode surface is simulated in the model as the NI emission flux from 300 to 3000 A m^{-2} randomly distributed along the surface representing different Cs conditioning states in the source.

In order to speed-up the simulation, ONIX code is parallelized via Message Passing Interface (MPI) using full domain and particles decomposition techniques. Typical runs with 30×10^6 macro particles, each representing 5×10^5 real particles take from 7 to 14 days on 20 CPUs.

3. Results and discussion

3.1. Meniscus formation

The positive extraction potential ($V_{ext} = 25$ kV) applied to the puller electrode attracts both negative species namely hydrogen negative ions and electrons and repels positively charged particles. Positive ions form a semi-spherical structure called meniscus. The meniscus position (defined also as boundary between the plasma and the beam, where the potential is ≈0 V) and the depth of its curvature (with respect to the extraction electrode plane) play an important role for the NI beam formation and the further characteristics of the beam optics since it defines the velocity starting angle of each extracted particle and its direction during the first moments of acceleration. Moreover, the extraction of NI independently of the production channel, on the surface or in the plasma volume, is governed by the meniscus shape, which in-turn depends on the local density of charged species. The extraction potential, geometry of the extraction aperture, plasma density and plasma composition also influence the meniscus shape.

The self-consistent meniscus formation for IS01 and IS02 extraction systems are shown in figure 6(A.a)—H^+ initial position for IS01 along the whole simulation domain, (A.b)—H^+ steady state distribution for IS01 zoomed close to the extraction electrode, (B.a)—H^+ initial position for IS02 along the whole simulation domain, (B.b)—H^+ steady state distribution for IS02 zoomed close to the extraction electrode. One can see how positive ions are self-consistently organized in the meniscus structure close to the extraction electrode (figures 6(A.b), (B.b)). However, the meniscus position and its width strongly depend on the shape of the extraction electrode. In the case of IS01 (cylindrical aperture) the deepest meniscus curvature point is located at a distance ≈2 mm from the beginning of the extraction electrode plane (figure 6(A.b)) and it is not penetrating inside the aperture. Changing the extraction aperture only as it is the case of IS02 (conical double chamfered), the deepest meniscus curvature point moves closer to the extraction electrode plane (~1.8 mm; figure 6(B.b)) with onset points at the distance ~0.5 mm from the extraction electrode 'knife' point ($x = 23.3$ mm). Similar behavior has been observed for the molecular positive ions, H_2^+ and H_3^+ (not shown).

3.2. Plasma screening

The spatial distribution of the electrostatic potential at the beginning of the simulation ($t = 0$) and at the quasi steady state regime ($t \approx 1$ μs) are shown in figure 7. In the initial state the external electric field deeply penetrates inside the plasma chamber in both systems IS01 and IS02 (figures 7(A.a) and (A.b)). However, when the sheath develops, the plasma screening occurs, the potential isolines are pushed towards the extraction electrode. For instance, the potential isoline of 100 V is shifted from $x \approx 14$ mm when the simulation starts to $x \approx 23$ mm when the steady state of IS01 is achieved (from figures 7(A.a) to (B.a)); and from $x \approx 15$ mm to $x \approx 23$ mm for the IS02 system (from figures 7(A.b) to (B.b)). Therefore, in quasi steady state regime the potential isoline of 100 V is located at the entrance plane of the extraction aperture for both systems. The neutrality of the systems is maintained at the bulk plasma region ($0 < x < 12.3$ mm) which plays the role of a

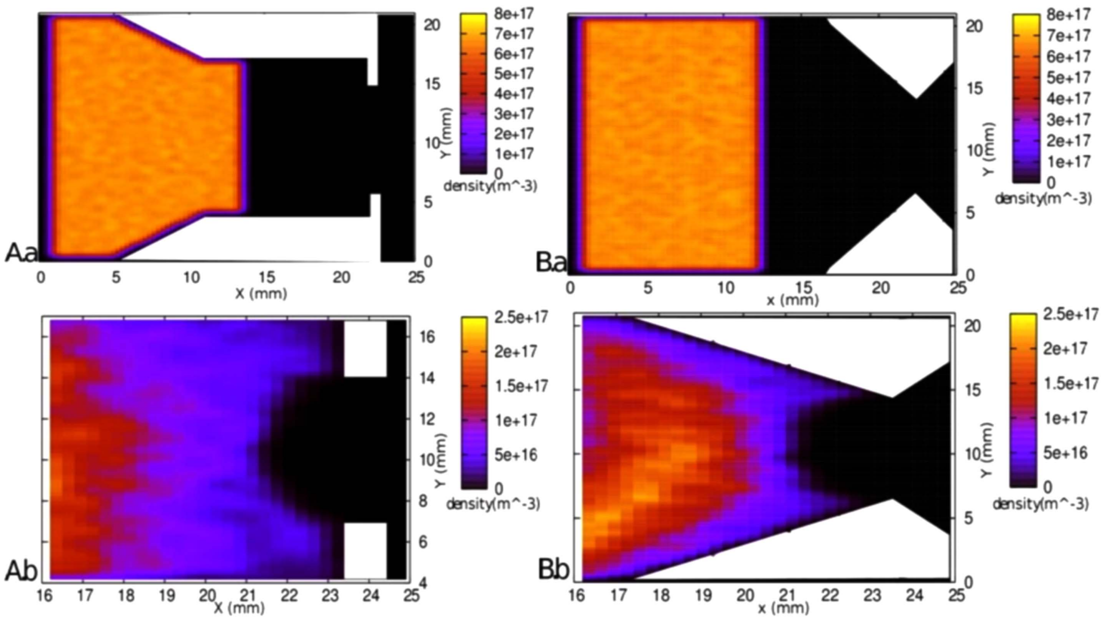

Figure 6. Positive atomic ion (H^+) density distributions in the mid-plane of the aperture ($z = 10$ mm). Left column (A) represents the IS01 and right column (B) the IS02 beam formation area. Row (a)—initial H^+ density used for input in ONIX, (b)—distribution of H^+ at steady state.

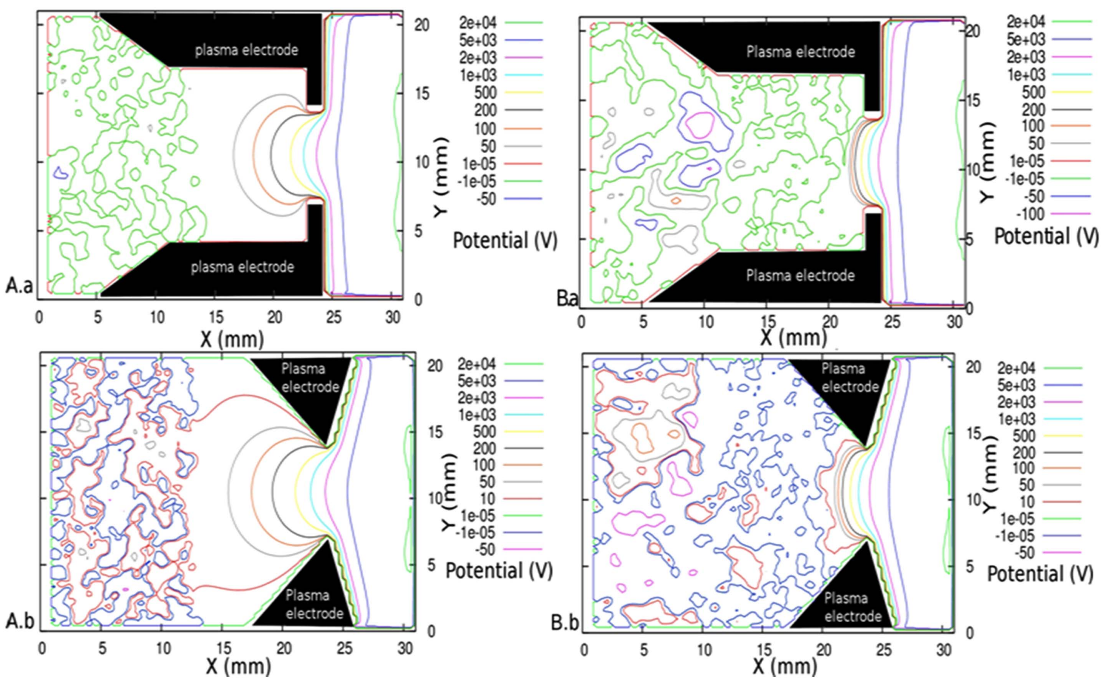

Figure 7. 2D potential distribution in the mid-plane of the aperture ($z = 10$ mm) at the beginning of the simulation (column A, $t = 0$) and once the quasi-steady state regime is achieved (column B $t > 1$ μs), for IS01—row (a) and IS02 row (b) extraction systems.

reservoir. The potential is constant or slowly varies in most of the volume inside the reservoir. Similar meniscus studies were also performed [15, 25, 26] but for fusion sources.

The importance of the plasma screening effect on the NI extraction can be easily seen in figure 8, where the NI trajectories are represented for two cases, for the extraction of the source IS01. First, a few test NIs are released without velocity in the plane perpendicular to the beam axis (at $x = 20$ mm), in front of the aperture under vacuum (i.e., the electric field is calculated as solution of Laplace equation, figure 8(a)) and with the electric field obtained once the meniscus is formed, i.e., in the quasi steady state taking into account the plasma effect (figure 8(b)). Without plasma (vacuum), all NIs are extracted (figure 8(a)) due to the deep penetration of the

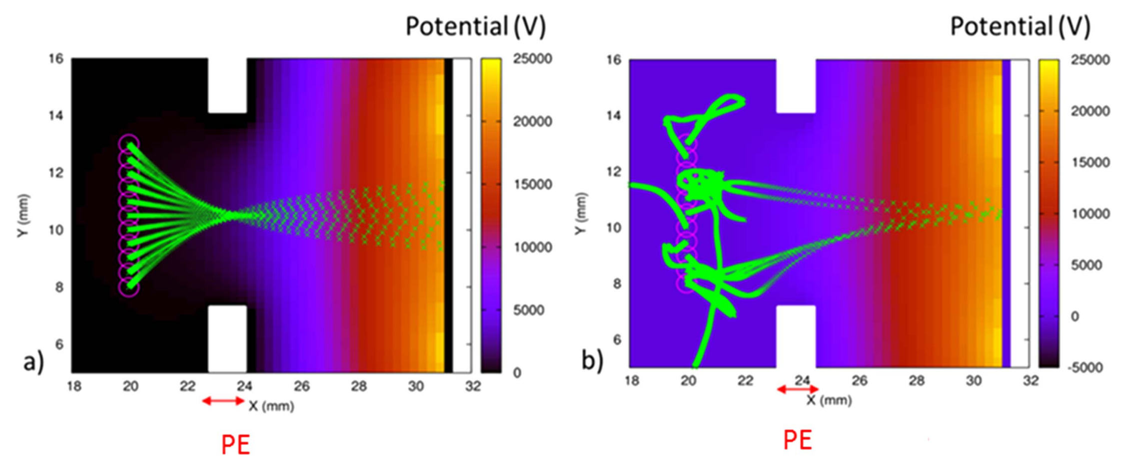

Figure 8. Trajectories of a bunch of NIs released without initial velocity close to the aperture in the IS01 source (a) in vacuum and (b) in the electric field obtained after the meniscus formation, as consequence of the plasma screening. The plasma electrode is indicated (PE).

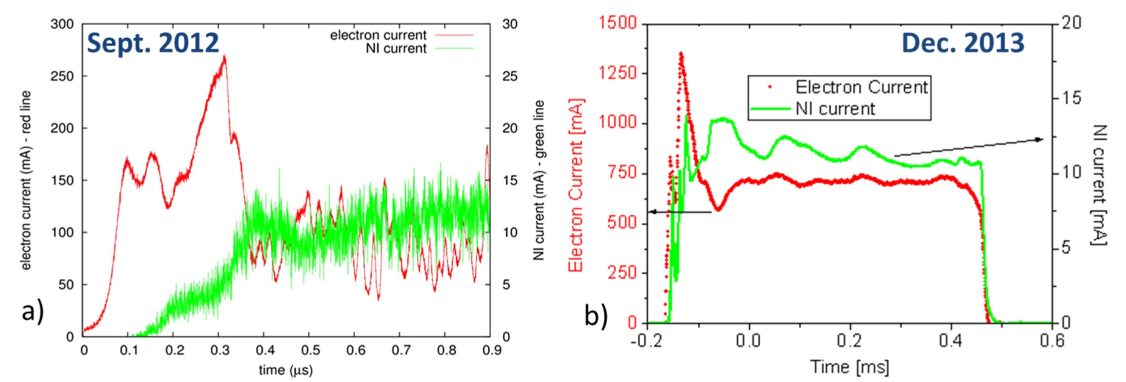

Figure 9. Time evolution of the extracted NI (green line) and co-extracted electron (red line) current for the IS01 extraction systems (a) calculated by ONIX simulation using 25 kV extraction potential and (b) measured at CERN.

extraction potential in this region, as shown in figure 7(A.a). On the contrary, when the plasma screening occurs most of the negative ions have complex unpredictable trajectories starting from this plane. Some of them move back towards the plasma chamber, while some others continuously turn around at the same place (as being electrostatically trapped) and only a small fraction of them is extracted through the aperture (figure 8(b)).

3.3. Simulation of extracted NI and electron current from IS01 negative ion source

ONIX follows all the plasma species in 3D inside the simulation domain. Hence, it is able to compute the amount of co-extracted electrons from the plasma, which pass the aperture in spite of the magnetic filter field. The extracted current is accounted for when the electrons or NI cross the right boundary of the simulation domain. The typical evolution of the extracted negative ions and co-extracted electron currents for IS01 system is shown in figure 9(a). One can see that the electron current grows very fast at the beginning, because the extraction potential is not screened yet. This growing continues until 0.3 μs. At this time, the screening of the extraction potential starts being efficiently, reducing the fraction of the co-extracted electrons. After this transitory phase, the NI and electron currents stabilize and the system evolves to reach a quasi-steady state after 0.6 μs.

The asymptotic value numerically estimated for the extracted NI current is ≈12 mA (figure 9(a) green line). The value of co-extracted electron current (figure 9(a), red line) is ≈90 mA. Therefore, the value of the electron/NI current ratio is about 7.5. These previously predicted simulation results were benchmarked with experimental measurements performed on IS01 NI source, shown in figure 9(b). Let us note that the simulations were performed in September 2012 before the measurements, performed one year later, in December 2013.

Analyzing the two panels (a) and (b) of figure 9, we found that the IS01 measured NI current ($I_{H^-,\mathrm{exp.}} \approx$ 12 mA) is in good agreement with the simulation one ($I_{H^-,\mathrm{ONIX}} \approx 10.6 \pm 1.9$ mA). This shows that ONIX is

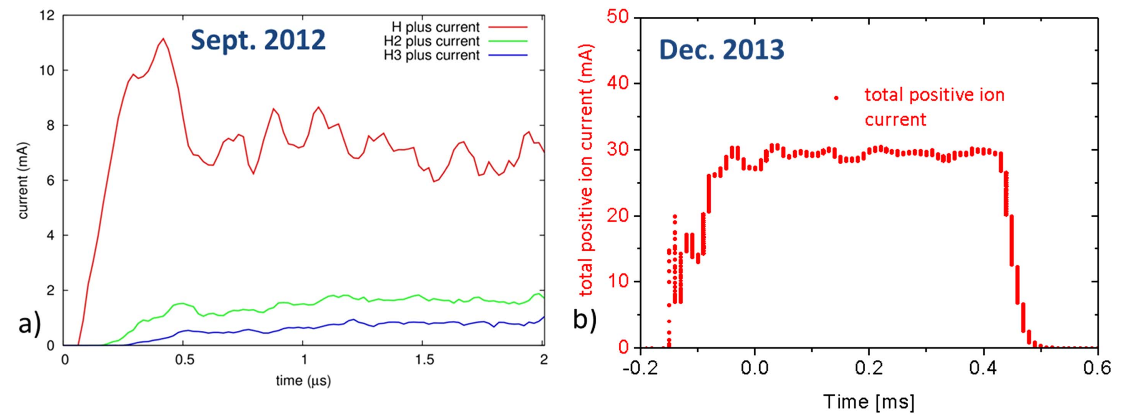

Figure 10. Time evolution of the extracted positive ion current for the IS01 extraction systems from the ONIX simulation (a) and from the experimental measurements (b).

able to extract NI from the plasma volume, without considering any mechanism for NI surface production, if the plasma parameters introduced in the *reservoir* region are close to experimental values. However, the co-extracted electron current is much higher in experiments ($I_{e,\mathrm{exp.}} \approx 600$ mA) in comparison to the simulations ($I_{e,\mathrm{ONIX}} \approx 89.8 \pm 26$ mA). Such discrepancy could be explained by the lower plasma density ($n_0 = 10^{18}\ \mathrm{m}^{-3}$) used as input in ONIX simulation due to the lack of experimental data in 2012, but also to the stability limit of the model (certainly below $2 \times 10^{18}\ \mathrm{m}^{-3}$ for the plasma density), in spite of the numerous improvements detailed in section 2.

A very long conditioning time was observed during the tests in the presence of O-rings. The IS02 prototype, once equipped with metallic sealing of the plasma chamber, was operated in volume production with a different puller geometry but similar field strength and reached after one month an electron to ion ratio of 18. The concentration of impurities such as water vapor for instance are not included in the simulation.

A time averaged saturation plasma density of up to $n_0 = 4 \times 10^{19}\ \mathrm{m}^{-3}$ [2] is measured above 60 kW RF-power; the view port used for the measurement points at the center of the plasma; this value is typically a factor 5 higher than in the bulk plasma region. The density of 1-2 $\times\ 10^{18}\ \mathrm{m}^{-3}$ correspond to an RF-heating power of the order of 15 kW and represents the highest plasma density that can be simulated, being sure that the steady state is reached.

In order to reveal the influence of the plasma density on the co-extracted electron current, additional simulations were performed with three different values of plasma density: (1) $n_0 = 5 \times 10^{17}\ \mathrm{m}^{-3}$, (2) $n_0 = 1 \times 10^{18}\ \mathrm{m}^{-3}$, (3) $n_0 = 2 \times 10^{18}\ \mathrm{m}^{-3}$. Increasing plasma density two times, from $n_0 = 1 \times 10^{18}\ \mathrm{m}^{-3}$ to $n_0 = 2 \times 10^{18}\ \mathrm{m}^{-3}$, the co-extracted electron current increases by about 1.5, from $I_{e,\mathrm{ONIX}} \approx 90$ mA to $I_{e,\mathrm{ONIX}} \approx 130$ mA, while the extracted NI current grows only marginally.

When the simulations were performed in 2012 we knew that the experimental setup enables inversion the polarity of the extraction potential in order to extract positive ions (PI). It was decided to simulate by means of ONIX also the protons extraction and compare the obtained results with future measured experimental data. For this test we kept the plasma density $n_0 = 10^{18}\ \mathrm{m}^{-3}$ with positive ion ratio: $S_{H^+}/S_{H_2^+}/S_{H_3^+} = 0.7/0.2/0.1$ into the source. The time evolution of the positive ion extracted current is shown in figure 10(a). The total simulated extracted PI current is $I_{PI} \approx 10$ mA. The measured total positive ion current at the exit of IS01 source one year after the simulations is about 3 times higher $I_{PI} \approx 30$ mA. This factor is related to the 45 kW radio-frequency power used in this experiment, that provides higher plasma density than the one was used in the simulation ($n_0 = 10^{18}\ \mathrm{m}^{-3}$ in the filter field region).

3.4. Simulation of extracted NI and electron current from IS02 negative ion source

The challenge of these CERN NI sources is to provide 80 mA of negative ions to Linac4. In order to increase negative ion production yield, Cs vapor is injected in the source; covering the inner surface of the Mo-plasma electrode, it provides a low work function ($W_{Cs} \approx 2.1$ eV). Cs atoms cover all the chamber surfaces, negative ions are effectively produced via gas atomic or positive ion conversion after their interaction with the cesiated molybdenum plasma electrode, as described in the Introduction section [10].

The amount of the surface produced NI can be theoretically calculated from the conversion yield, which could reach up to 20 percent [27], and the number of impinging neutrals/positive ions [28]. Because of the lack of precise values of the atomic hydrogen density in the CERN source and the thickness of the Cs layer covering the extraction electrode that determines Cs work function, several runs have been performed as parametric

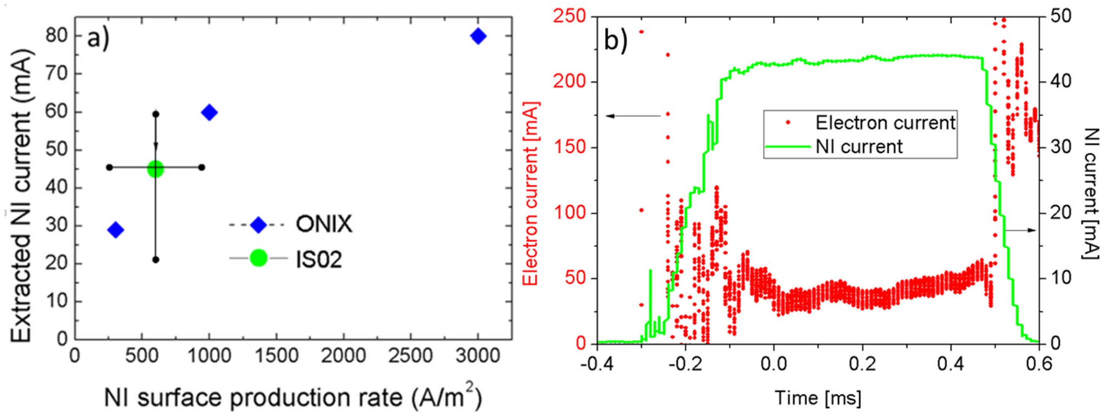

Figure 11. (a) Negative ion extracted current versus the NI emission rate from the surface for IS02 source simulated by ONIX (blue diamond). The cesiated surface IS02 measurement is placed on the same graph (green circle at 45 mA with a line indicating the experimental range of 20–60 mA). The horizontal bar indicates the range of corresponding NI surface production rate (200–900 A m^{-2}). (b) 45 mA H$^-$ extracted NI and co-extracted electron current in IS02 (origin of green circle on figure 11(a)).

Table 1. Summary of the ONIX simulation for IS02, the plasma density is 1×10^{18} m^{-3}, the negative ion to electron ratio, the NI surface emission rate and the Cs$^+$ density are indicated. The mean value ± standard deviation of the NI current produced from the surface or form the volume and the co-extracted electron current are indicated.

Cs density m^{-3}	NI/e ratio %	NI emission rate A m^{-2}	H$^-$ current surface mA	H$^-$ current volume mA	e current mA
0	50/50	1000	54.9 ± 1.1	7.4 ± 1.6	41.4 ± 13.8
0	50/50	3000	69.5 ± 3.9	7.8 ± 2.2	76.7 ± 36.4
0	50/50	6500	63.5 ± 4.0	9.8 ± 2.6	75.8 ± 27.3
0	70/30	3000	69.3 ± 3.8	8.8 ± 2.3	37.1 ± 17.5
3.3×10^{15}	70/30	300	20.8 ± 2.2	7.9 ± 1.8	10.9 ± 6.5
1.3×10^{16}	70/30	1000	48.2 ± 3.2	8.6 ± 1.0	18.4 ± 18.3
3.8×10^{16}	70/30	3000	69.6 ± 3.7	7.9 ± 1.6	33.2 ± 32.1

study of the NI emission rate from the cesiated surface. NI emission rates lying from 300 to 3000 A m^{-2} were considered and the numerical results for IS02 system are presented in figure 11. However, before contaminating the source by the Cs vapor it was decided to check IS02 source performance for the NI production only due to the volume processes, as it was for IS01. The ONIX simulation results show that the NI extracted current for IS02 source in Cs free regime reaches about $I_{H^-,\mathrm{ONIX}} \approx 13$ mA and the co-extracted electron current is about $I_{e,\mathrm{ONIX}} \approx 80$ mA. These results are in good agreement with measurements $I_{H^-,\mathrm{exp.}} \approx 10$–20 mA for low power experiments $P_{RF} = 20$ kW ([2], figure 8).

Figure 11(a)) presents the extracted NI current versus the negative ion emission rate from the extraction electrode surface. The NI emission rate in the simulation represents the H$^-$ production yield of the cesiated surface. A Cs$^+$ ion density in the bulk plasma region is reported in [29]; we therefore associated Cs$^+$ ion densities to the surface emission rates: 300, 1000 and 3000 A m^{-2} and $n_{Cs^+} = 3.3 \times 10^{15}$, 1.3×10^{16} and 3.8×10^{16} m^{-3}, respectively. The trend of NI extracted current is saturating with increasing emission rate. The reason of such limitation is due to the well-described double layer structure formation [11, 15, 28] (negative potential well) in front of the plasma electrode that reflect an important amount of the surface produced NI back to the plasma electrode where they are destroyed. Increasing the emission rate, the effective surface of the conical aperture reduces, and the NI can be extracted only from a smaller and smaller area, close to the knife of the aperture leading to the NI current saturation [11].

The IS02 simulations are presented in table 1, the current of H$^-$ originating form surface emission is as expected clearly driven by the emission rate and saturates at 70 mA. The electron current depends on the electron to NI ratio and including Cs ions in the plasma did not significantly impact the extracted current.

The total extracted NI current varies from $I_{H^-,\mathrm{ONIX}} \approx 29$ mA for the NI surface emission rate of 300 A m^{-2} up to 80 mA for 3000 A m^{-2} (figure 11). The experimental results ([2], figure 8) spread out in the range of 20–60 mA depending of the RF-power and source conditioning. As an indication, 45 mA (figure 11(b)) of NI extracted current was positioned on the simulation trend line on figure 11(a)). Assuming that the plasma density would match the simulated one, this would, corresponds to a NI surface emission rate range of 200–1000 A m^{-2}, matching the theoretically estimated NI emission rate for fusion sources of 600 A m^{-2} [28]. Therefore, we observe similar order of magnitude between two different simulations (ITER and CERN cesiated surface sources) in terms of NI emission rate and as well between the ONIX simulation and measured H^- ion current.

4. Conclusions

The plasma property and extraction capability of both extraction systems (IS01, IS02), developed at CERN, were studied using a modified version of self-consistent 3D PIC MCC model ONIX with a single extraction aperture and without periodic boundary conditions. Simulations show the self-consistent positive ion meniscus formation in the vicinity of the extraction aperture and the plasma screening of the external extraction potential.

The extracted NI and co-extracted electron current were calculated for both IS01 and IS02 extraction systems for different plasma and source parameters. The simulated results were obtained prior to experiment and benchmarked with experimental data. Good agreement was found in term of the extracted NI current. The co-extracted electron current in most cases is smaller in the simulation than in the experiments. Such difference is partially explained by the difference of the electron density used in the simulation (10^{18} m^{-3}) in comparison to one measured in the experiments.

The NI surface production has been simulated for the IS02 extractor and a parametric study of the NI emission rate was performed. Assuming a NI surface emission rate of 600 A m^{-2} (theoretically estimated for the fusion NI sources [28]) the IS02 results perfectly fit on the trend line of the simulation.

In the future more precise plasma parameters will be available from the spectroscopy diagnostic installed around the plasma generator of the IS02 source test stand [22]. Simulations of the H_0 and protons fluxes in the plasma will provide more detailed information about NI emission rate from the cesiated plasma electrode surface. Using these data as input parameters in the ONIX code will allow to perform calculations with higher accuracy.

Acknowledgments

Useful discussions with all members of CERN Linac4 group are truly acknowledged.

References

[1] Arnaudon L *et al* 2006 *Linac4 Technical Design Report* Report No. CERN-AB-2006-084 ABP/RF, European organization for nuclear research CERN - AB department (http://project-spl.web.cern.ch/project-spl/documentation/l4tdr.pdf)
[2] Lettry J *et al* 2015 CERN's Linac4 H− sources: status and operational results *AIP Conf. Proc.* **1655** 03005
[3] Lettry J *et al* 2014 Status and operation of the Linac4 ion source prototyp *Rev. Sci. Instrum.* **85** 02B122
[4] Lettry J *et al* 2012 H- ion sources for CERN's Linac4 *AIP Conf. Proc.* **1515** 302–11
[5] Paoluzzi M M *et al* 2011 *AIP Conf. Proc.* **1390** 265–71
[6] Kronberger M *et al* 2011 *AIP Conf. Proc.* **1390** 255–64
[7] Janev R 1987 *Elementary Processes in Hydrogen–Helium* (Berlin: Springer)
[8] Bacal M *et al* 2006 *Nucl. Fusion* **46** S250
[9] Speth E *et al* 2006 *Nucl. Fusion* **46** S220
[10] Belchenko Y 1993 *Rev. Sci. Instrum.* **64** 1385
[11] Mochalskyy S *et al* 2012 *J. Appl. Phys.* **111** 113303
[12] Mochalskyy S *et al* 2010 *Nucl. Fusion* **50** 105011
[13] Ikeda K *et al* 2013 *New J. Phys.* **15** 103026
[14] Mochalskyy S *et al* 2015 *Nucl. Fusion* **55** 033011
[15] Mochalskyy S *et al* 2014 *Plasma Phys. Control. Fusion* **56** 105001
[16] Mochalskyy S *et al* 2013 *AIP Conf. Proc.* **1515** 31
[17] Kaasschieter E F *et al* 1988 *J. of Comput. and Appl. Math* **24** 265–75
[18] Gibou F *et al* 2002 *J. Comput. Physics* **176** 205–27
[19] Opera Simulation Software (http://operafea.com/)
[20] Birdsall C K and Langdon A B 1985 *Plasma Physics via Computer Simulation* (New York: McGraw-Hill)
[21] Courant R, Friedrichs K and Lewy H 1928 *Mathematische Annalen* **100** 3274
[22] Briefi S *et al* 2016 *Rev. Sci. Instrum.* **87** 02B104
[23] Mattei S *et al* 2013 *AIP Conf. Proc.* **1515** 386–93
[24] Schmitzer C *et al* 2012 *Rev. Sci. Instrum.* **83** 02A715
[25] Nishioka S *et al* 2014 *Rev. Sci. Instrum.* **85** 02A737
[26] Taccogna F *et al* 2013 *Plasma Sources Sci. Technol.* **22** 045019
[27] Rasser B *et al* 1982 *Surf. Sci.* **118** 697–710
[28] Wunderlich D *et al* 2009 *Plasma Sources Sci. Technol.* **18** 045031
[29] Fantz U *et al* 2006 *Nucl. Fusion* **46** S297–306